Modeling of the Characteristic Size of Drops in a Spray Produced by the Supersonic Gas Atomization Process

N. Apell*, I. V. Roisman, C. Tropea, J. Hussong
Institute for Fluid Mechanics and Aerodynamics, Technische Universität Darmstadt, Darmstadt, Germany
*Corresponding author: apell@sla.tu-darmstadt.de

Abstract
Liquid atomization using supersonic gas flows is a common process in many industrial applications, one example being the atomization of liquid metals. In the present experimental and analytical work, a modeling approach for the characteristic size of drops in sprays produced by means of supersonic gas atomization has been developed.
Local drop size distributions within the spray produced by a generic close-coupled atomizer operated with air have been obtained using the phase Doppler measurement technique. In order to investigate the importance of the liquid properties for the atomization process, water as well as two different aqueous glycerol solutions have been considered. No significant influence of the liquid dynamic viscosity on the drop size within the spray has been observed.
Employing the chaotic disintegration theory, a characteristic length scale has been derived as a function of the deformation Weber number. The corresponding liquid deformation velocity has been estimated by describing the formation of a shock wave in the gas stream during the initial interaction of a liquid volume and a supersonic gas flow.
Furthermore, a semi-empirical model based on the liquid Weber number has been proposed taking into account macroscopic effects at scales comparable to the size of the liquid jet. The correlation has been found to agree very well with the obtained experimental data.

Keywords
Supersonic gas atomization, close-coupled atomization, modeling, characteristic length scale

Introduction

The atomization of liquids by means of supersonic gas flows has many industrial applications and is becoming more and more economically relevant. This is especially true in the context of metal processing, where it is, for instance, used for the production of fine metal powders, which serve as the raw material for metal additive manufacturing employing the laser powder bed fusion process [1].
There is a variety of different atomizer configurations used in supersonic gas atomization, featuring various liquid and gas nozzle designs [3]. The specific atomizer design not only has a strong influence on the gas flow field but also on the interaction of gas and liquid flow and, therefore, on the resulting spray and particle size. However, common characteristics are very high local gas velocities and the formation of expansion as well as compression waves. For instance, in Figure 1a, a focusing Schlieren image of the gas-only flow field downstream of a generic close-coupled atomizer featuring a central liquid nozzle surrounded by a converging-diverging annular slit gas nozzle operated in underexpanded condition is shown, which has been taken by Luh et al. [2]. Local changes in gas density in vertical direction due to the formation of expansion as well as compression waves are clearly visible.
As a result, the interaction of gas and liquid flow is very complex, as can be seen in Figure 1b, which shows a still image of the multiphase flow for the same set point of operation. Consequently, existing models describing the characteristic size of drops produced by supersonic gas atomization are mostly empirical and, therefore, do not sufficiently capture the physics involved in the process. In contrast, in the following, a semi-empirical modeling approach partially based on physical phenomena is proposed.

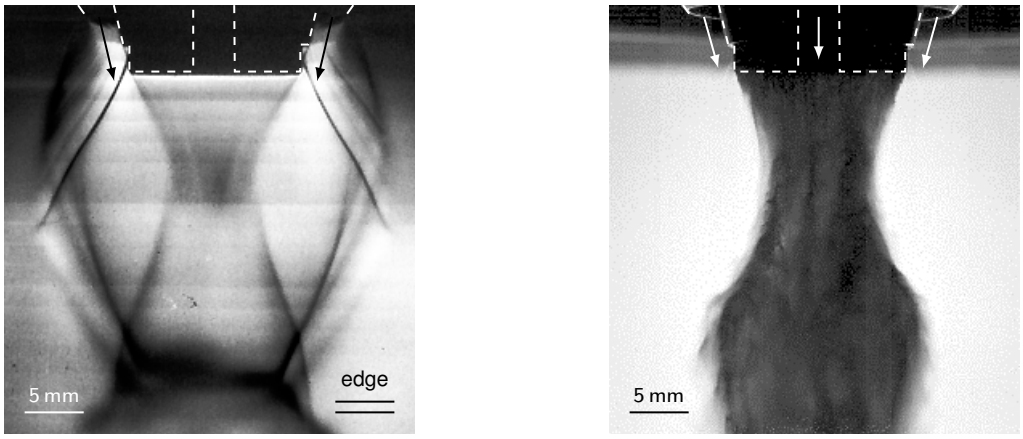

(a) (b)

Figure 1. Visualization of the flow field downstream of a close-coupled atomizer (the geometry of the liquid nozzle and the surrounding annular slit gas nozzle are indicated using dashed white lines; the respective fluid flows are illustrated using arrows): a) focusing Schlieren image of the gas-only flow (air) by Luh et al. [2], and b) still image of the multiphase flow (water and air).

Liquid Properties Governing Atomization

While liquid atomization is certainly significantly influenced by the properties of the specific gas flow involved, especially when considering effects of compressibility, it is well known that the process is usually governed by liquid dynamic viscosity μ_l and surface tension σ [4–6]. Correspondingly, the regimes characterizing atomization are described using Reynolds number and Weber number. For supersonic gas atomization, however, the influence of liquid dynamic viscosity μ_l and surface tension σ is not known and, therefore, requires further investigation.
In order to determine whether the liquid dynamic viscosity μ_l has a significant effect on the drop size resulting from supersonic gas atomization, size distributions produced by means of a generic close-coupled atomizer operated with air have been obtained for different liquids using the phase Doppler measurement technique. A brief overview of the measurement setup as well as the data analysis has been given by Apell et al. [7].

Table 1. Physical fluid properties of the three liquids investigated at a temperature of 20 °C and a pressure of 1013.25 hPa.

Property	Water	20 m% Glycerol	40 m% Glycerol
Density ρ_l [kg m^{-3}]	998	1051	1103
Dynamic viscosity μ_l [mPa s]	1.00	1.74	3.68
Surface tension σ [mN m^{-1}]	72.7	71.0	69.3

In detail, water as well as aqueous glycerol solutions of two different mass fractions (20 m% and 40 m%) have been considered. For a temperature of 20 °C and a pressure of 1013.25 hPa, the physical fluid properties of the three liquids are given in Table 1. They have been calculated following recommendations from the IAPWS [8–10], the VDI [11] and using the approach by Cheng [12]. As can be seen, the three liquids show a significant difference in terms of dynamic viscosity μ_l.
Drop size distributions in different positions within the spray have been measured for varying gas stagnation pressures $p_\mathrm{t,g}$ and liquid mass flow rates $\dot{m}_\mathrm{l}$. In Figure 2a, the difference in number median diameter d_N50 between water and the two aqueous glycerol solutions is shown as a function of the gas stagnation pressure $p_\mathrm{t,g}$, including corresponding 95 % confidence intervals. Here, measurements have been performed in the center of the spray and the liquid mass flow rate has been set to $\dot{m}_\mathrm{l} = 6\,\mathrm{kg\,min^{-1}}$, however, the results are representative for the entire experimental study. As can be seen, a significant influence of the glycerol mass fraction on the drop size cannot be identified. Similar results have been found for the number based diameter interquartile range $IQR_{d,\mathrm{N}}$, which is a measure of the dispersion of the drop size, as

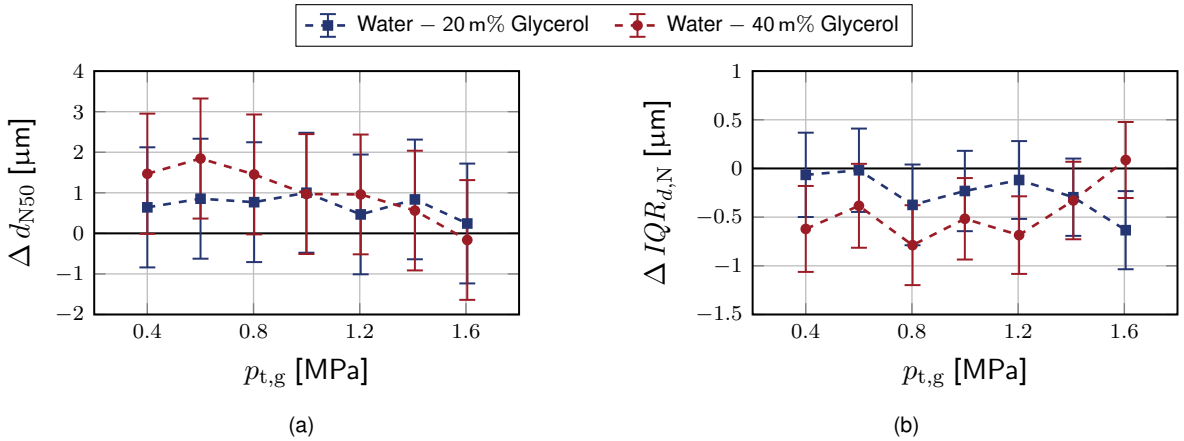

Figure 2. Difference in drop size characteristics in the center of the spray as a function of the gas stagnation pressure $p_{t,g}$ for a liquid mass flow rate of $\dot{m}_l = 6\,\mathrm{kg\,min^{-1}}$: a) number median diameter d_{N50}, and b) number based diameter interquartile range $IQR_{d,N}$.

can be seen in Figure 2b.
The experimental results suggest that the influence of the liquid dynamic viscosity μ_l on the size of the drops in the spray is negligibly small. Therefore, surface tension σ is assumed to be dominant in supersonic gas atomization and will be considered further in the following. This seems reasonable, since in practical applications initial Ohnesorge numbers Oh based on the liquid nozzle diameter are usually much smaller than one.

Chaotic Disintegration Model for the Breakup of a Deforming Liquid Element

For the liquid breakup model, the disintegration is assumed to be of chaotic nature. This seems reasonable considering the very high relative velocities and short time scales involved in the rather violent process of the liquid jet fragmentation.

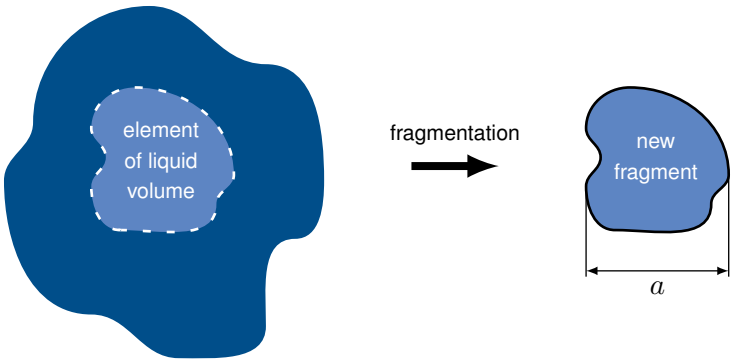

Figure 3. Schematic illustration explaining the principle of the chaotic disintegration theory.

The main idea behind the chaotic disintegration theory, which has been detailed by, for instance, Yarin [13], is schematically shown in Figure 3. Here, a small element of a liquid volume is considered. The element has the characteristic size a and separates from the liquid volume due to its fast deformation caused by, for instance, a supersonic gas flow. After the disintegration the element forms a new fragment. The process of disintegration is governed by the kinetic energy E_K of the element. Part of this energy is transformed during the creation of the surface of the new fragment into the surface energy E_σ. Both energies are estimated as

$$E_K \sim \rho_l a^3 \left(a\dot{\gamma}\right)^2, \quad E_\sigma \sim \sigma a^2, \tag{1}$$

where $\dot{\gamma}$ is the local effective strain rate of the liquid element and ρ_l is the liquid density. It is required that $E_K \geq E_\sigma$ holds. The time scale of the separation of the element from the liquid volume leading to fragment formation is extremely short. Therefore, the energy loss due to the

viscous dissipation in the element is negligibly small in comparison with the kinetic energy E_{K}. This assumption is in accordance with the experimental results demonstrating the negligible role of the liquid dynamic viscosity μ_{l} discussed above.
The smallest possible fragment is obtained in the case of the entire kinetic energy E_{K} of deformation transforming into the surface energy E_σ of the new fragment, that is, $E_{\mathrm{K}} = E_\sigma$. This condition in combination with Equation (1) yields an expression for the smallest possible fragment size:

$$a \sim \left[\frac{\sigma}{\rho_{\mathrm{l}}\dot{\gamma}^2}\right]^{1/3}. \tag{2}$$

Now, the chaotic disintegration of a specific liquid volume having the initial length scale d_0 is considered. The characteristic deformation velocity of the volume is assumed to be u_{def}. Therefore, the effective strain rate $\dot{\gamma}$ can be estimated as $\dot{\gamma} \sim u_{\mathrm{def}}/d_0$. Finally, using Equation (2), the characteristic size a of the fragments after the disintegration of the liquid volume of initial size d_0 can be expressed in the form

$$a = d_0\, We_{\mathrm{def}}^{-1/3}, \quad We_{\mathrm{def}} = \frac{\rho_{\mathrm{l}} d_0 u_{\mathrm{def}}^2}{\sigma}, \tag{3}$$

where We_{def} is the deformation Weber number.

Liquid Volume Deformation by a Supersonic Flow

The deformation velocity u_{def} needs to be determined taking into account the supersonic gas flow. The basic flow setup considered here is shown in Figure 4. A liquid volume having the initial length scale d_0 is suddenly exposed to a supersonic gas flow. The liquid is assumed to be incompressible and its liquid density, dynamic viscosity and surface tension are denoted as ρ_{l}, μ_{l} and σ, respectively. Furthermore, the gas is assumed to be calorically perfect with ratio of specific heats κ and its flow to be inviscid, characterized by the velocity u_{g}, the pressure p_{g} and the density ρ_{g}.

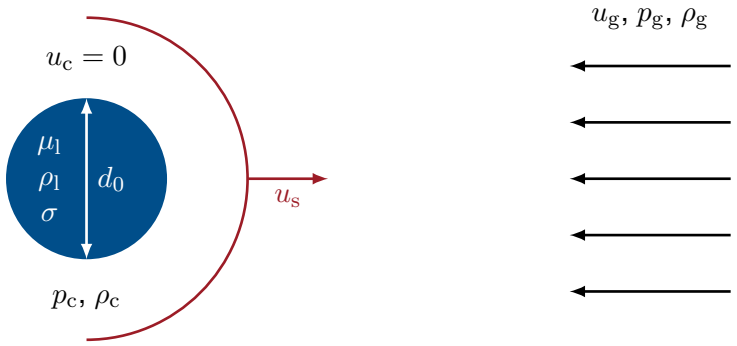

Figure 4. Schematic illustration of the initial interaction between a liquid volume and a supersonic gas flow.

Due to the compressible nature of the described supersonic gas flow, an adiabatic shock wave forms at the liquid surface during the initial interaction and propagates upstream into the gas flow with velocity u_{s}. As a simplification, the flow across the shock wave is assumed to be one-dimensional, that is, a normal shock wave is considered. Hence, according to, for instance, Anderson [14], the conservation equations for mass, momentum and energy across the shock wave can be formulated:

Mass:
$$\rho_{\mathrm{c}} u_{\mathrm{s}} = \rho_{\mathrm{g}}(u_{\mathrm{g}} + u_{\mathrm{s}}) \tag{4}$$

Momentum:
$$p_{\mathrm{c}} + \rho_{\mathrm{c}} u_{\mathrm{s}}^2 = p_{\mathrm{g}} + \rho_{\mathrm{g}}(u_{\mathrm{g}} + u_{\mathrm{s}})^2 \tag{5}$$

Energy:
$$\frac{\kappa}{\kappa - 1}\frac{p_{\mathrm{c}}}{\rho_{\mathrm{c}}} + \frac{u_{\mathrm{s}}^2}{2} = \frac{\kappa}{\kappa - 1}\frac{p_{\mathrm{g}}}{\rho_{\mathrm{g}}} + \frac{(u_{\mathrm{g}} + u_{\mathrm{s}})^2}{2} \tag{6}$$

Here, it is important to note that the velocity of the compressed gas u_c downstream of the shock wave is assumed to be zero. The set of Equations (4) to (6) can be solved algebraically for the pressure difference Δp across the shock wave as a function of the gas quantities:

$$\Delta p = p_\mathrm{c} - p_\mathrm{g} = \frac{1}{4}\left\{\rho_\mathrm{g}\left(\kappa+1\right)u_\mathrm{g}^2 + \rho_\mathrm{g}^{1/2}u_\mathrm{g}\left[16\kappa p_\mathrm{g} + \left(1+\kappa\right)^2\rho_\mathrm{g}u_\mathrm{g}^2\right]^{1/2}\right\}. \tag{7}$$

Equation (7) is an interesting result, since it allows for estimating the pressure difference Δp solely from quantities characteristic for the supersonic gas flow without requiring knowledge of the shock velocity u_s and the compressed gas state.
Next, using Bernoulli's equation inside of the liquid volume, an approximation for the deformation velocity u_def of the liquid volume based on the pressure difference Δp across the shock wave can be found:

$$u_\mathrm{def} \approx \left(\frac{2\Delta p}{\rho_\mathrm{l}}\right)^{1/2}. \tag{8}$$

Here, it has to be noted that the Laplace pressure due to the surface curvature is neglected. Considering typical initial length scales d_0 characteristic for supersonic gas atomization, that is, for instance, liquid nozzle diameters, this simplification appears to be reasonable.
Finally, Equations (7) and (8) serve as a basis for evaluating the deformation Weber number We_def introduced in Equation (3):

$$We_\mathrm{def} = \frac{\rho_\mathrm{l} d_0 u_\mathrm{def}^2}{\sigma} = \frac{2\Delta p d_0}{\sigma}. \tag{9}$$

Similarly, the deformation Reynolds number Re_def can be introduced:

$$Re_\mathrm{def} = \frac{\rho_\mathrm{l} d_0 u_\mathrm{def}}{\mu_\mathrm{l}} = \frac{d_0\left(2\Delta p\rho_\mathrm{l}\right)^{1/2}}{\mu_\mathrm{l}}. \tag{10}$$

As a result, the condition $Re_\mathrm{def} \gg 1$ determines whether the assumption of the disintegration process being governed solely by the deformation Weber number We_def is justified.

Experimental Validation

Supersonic gas atomization is an extremely complicated process governed by various mechanisms at different length scales. So far, the characteristic length scale a has been derived, which needs to be compared to the characteristic size of drops in an actual spray produced by means of supersonic gas atomization. This has been done by performing phase Doppler measurements in various positions within the water spray produced by a generic close-coupled atomizer operated with air. A wide range of set points of operation has been covered, that is, the gas stagnation pressure $p_\mathrm{t,g}$ as well as the liquid mass flow rate $\dot{m}_\mathrm{l}$ has been varied systematically.
Additionally, for every set point of operation considered, the characteristic length scale a has been calculated. The necessary gas quantities characterizing the supersonic gas flow have been obtained from simulations of the gas-only flow field performed by Vogl et al. [15] for the identical atomizer geometry. In detail, the gas quantities have been averaged over the width of the gas jets in the position where the first interaction between gas and liquid takes place. Furthermore, for the initial length scale d_0 the liquid nozzle diameter has been employed. As a result, the deformation Reynolds number Re_def has been found to be larger than 10^5 for every set point of operation, justifying the neglect of the liquid dynamic viscosity μ_l.
In Figure 5a, the calculated characteristic length scale a is shown as a function of the gas stagnation pressure $p_\mathrm{t,g}$ for four different constant liquid mass flow rates $\dot{m}_\mathrm{l}$. As can be seen, an increasing gas stagnation pressure $p_\mathrm{t,g}$ results in a decreasing characteristic length scale a, with the sensitivity slightly decreasing as well. This result is in good agreement with experimental data for the particle size reported by, for instance, Urionabarrenetxea et al. [16]. At the

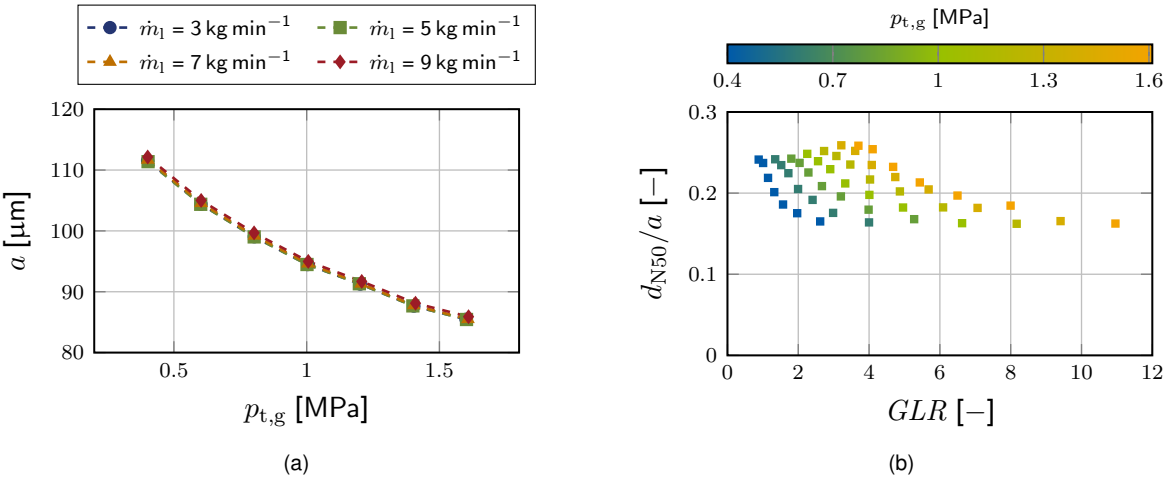

Figure 5. Calculated characteristic length scale a: a) influence of the set point of operation, and b) comparison with the measured number median diameter d_N50 as a function of the gas-to-liquid ratio GLR.

same time, the liquid mass flow rate $\dot{m}_\mathrm{l}$ does not seem to have an effect on the characteristic length scale a. However, experimental results have already suggested that the liquid mass flow rate $\dot{m}_\mathrm{l}$ is indeed a sensitive parameter in determining the drop size [7].
In purely empirical models, this discrepancy is often resolved by introducing the ratio of the fluid mass flow rates, also called gas-to-liquid ratio GLR, as a parameter characterizing the set point of operation on a macroscopic scale [17]. However, as can be seen in Figure 5b, where the ratio of the measured number median diameter d_N50 and the calculated characteristics length scale a is shown as a function of the gas-to-liquid ratio GLR, for the proposed modeling approach there is no obvious correlation. This is in accordance with results by, for instance, Urionabarrenetxea et al. [16], questioning the use of the gas-to-liquid ratio GLR for describing the drop size.

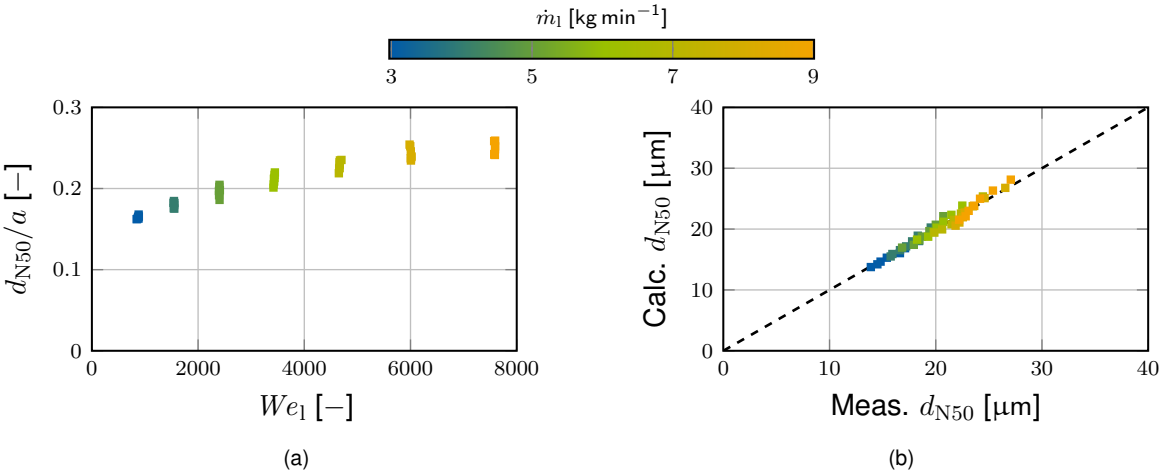

Figure 6. Characteristic length scale a as a function of the set point of operation: a) comparison with the measured number median diameter d_N50 as a function of the liquid Weber number We_l, and b) comparison of measured and calculated number median diameter d_N50.

On the other hand, promising results have been obtained when instead introducing the liquid Weber number $We_\mathrm{l} = \rho_\mathrm{l} u_\mathrm{l}^2 d_0/\sigma$ as a parameter governing the macroscopic operational parameters. Here, u_l is the liquid exit velocity of the liquid nozzle. The relationship between the liquid Weber number We_l and the ratio of the measured number median diameter d_N50 and the calculated characteristic length scale a is shown in Figure 6a, revealing an improved correlation. Finally, from Figure 6a a semi-empirical correlation for the number median diameter in the form

$$d_{\mathrm{N50}} = \alpha\, a\, We_{\mathrm{l}}^{\beta} \tag{11}$$

has been obtained by introducing two constants, α and β, as fitting parameters, where a is defined in Equation (3). The best fit for the experimental data yields the following result:

$$d_{\mathrm{N50}} = 0.04\, d_0\, We_{\mathrm{def}}^{-1/3}\, We_{\mathrm{l}}^{1/5}\,. \tag{12}$$

A comparison of the measured and the calculated number median diameter d_{N50} using Equation (12) is shown in Figure 6b. As can be seen, the agreement is very good over the entire range of set points of operation. In fact, the root mean squared error has been found to be as small as $0.6\,\mu\mathrm{m}$, which is comparable to the measurement uncertainty of the phase Doppler measurement system.

Summary and Conclusions

The characteristic size of drops within the spray produced by means of supersonic gas atomization has been investigated experimentally and analytically.

Measurements of the local drop size generated by a generic close-coupled atomizer have been performed employing the phase Doppler measurement technique. Data obtained for water as well as two different aqueous glycerol solutions suggests that the liquid dynamic viscosity μ_{l} does not have a significant influence on the drop size. Consequently, supersonic gas atomization has been assumed to be governed by surface tension effects.

The chaotic disintegration theory has been used to formulate an expression for the characteristic length scale a based on the deformation Weber number We_{def}. Furthermore, assuming the formation of a shock wave during the initial interaction of a liquid volume and a supersonic gas flow to be the main mechanism governing supersonic gas atomization, an approximation for the characteristic liquid deformation velocity u_{def} has been derived.

Analysis of the experimental data in terms of drop size has shown that not only the shock-liquid interaction but also the macroscopic properties of the liquid flow have a significant influence on the atomization result. As part of this study, these influences have been accounted for by introducing the liquid Weber number We_{l}. A semi-empirical correlation for the drop size has been formulated, which includes the characteristic length scale a as well as the liquid Weber number We_{l}. Agreement with the experimental data has been shown to be very good.

Future work will focus on further validating the developed model using experimental data obtained for various liquids having different surface tension σ. Additionally, optical measurement techniques will be used to improve the understanding of the influence of macroscopic operational parameters on the atomization process and to further motivate the usage of the liquid Weber number We_{l}.

Acknowledgements

The authors gratefully acknowledge the Indo-German Science & Technology Centre (IGSTC) for the financial support of the project “Metal Powder Production for Additive Manufacturing” (PPAM), funding code 01DQ19005A.

Nomenclature

α, β	Fitting parameters [$-$]	$IQR_{d,\mathrm{N}}$	Diameter interquartile range [m]
Δp	Pressure difference [Pa]	$\dot{m}_{\mathrm{l}}$	Liquid mass flow rate [kg s^{-1}]
$\dot{\gamma}$	Strain rate [s^{-1}]	Oh	Ohnesorge number [$-$]
κ	Ratio of specific heats [$-$]	p_{c}	Compressed gas pressure [Pa]
μ_{l}	Liquid dynamic viscosity [Pa s]	p_{g}	Gas pressure [Pa]
ρ_{c}	Compressed gas density [kg m^{-3}]	$p_{\mathrm{t,g}}$	Gas stagnation pressure [Pa]
ρ_{g}	Gas density [kg m^{-3}]	Re_{def}	Deformation Reynolds number [$-$]

ρ_l	Liquid density [kg m^{-3}]	u_c	Compressed gas velocity [m s^{-1}]
σ	Surface tension [N m^{-1}]	u_def	Deformation velocity [m s^{-1}]
a	Characteristic length scale [m]	u_g	Gas velocity [m s^{-1}]
d_0	Initial length scale [m]	u_l	Liquid velocity [m s^{-1}]
d_N50	Number median diameter [m]	u_s	Shock velocity [m s^{-1}]
E_K	Kinetic energy [J]	We_def	Deformation Weber number [$-$]
E_σ	Surface energy [J]	We_l	Liquid Weber number [$-$]
GLR	Gas-to-liquid ratio [$-$]		

References

[1] Yang, L., Hsu, K., Baughman, B., Godfrey, D., Medina, F., Menon, M., Wiener, S., 2017, Additive Manufacturing of Metals: The Technology, Materials, Design and Production, Springer Series in Advanced Manufacturing, Springer International Publishing, Cham and s.l.

[2] Luh, M. F., Vogl, N., Odenthal, H.-J., Roisman, I. V., Tropea, C., 2018, in Institute for Liquid Atomization and Spray Systems, ed., Proceedings of the 14th International Conference on Liquid Atomization & Spray Systems, p. 390.

[3] Henein, H., Uhlenwinkel, V., Fritsching, U., eds., 2017, Metal Sprays and Spray Deposition, Springer International Publishing, Cham.

[4] Crowe, C. T., 2005, Multiphase Flow Handbook, CRC Press.

[5] Ashgriz, N., ed., 2011, Handbook of Atomization and Sprays: Theory and Applications, Springer, New York.

[6] Lefebvre, A. H., McDonell, V. G., 2017, Atomization and Sprays, CRC Press, New York, 2nd revised ed. edition.

[7] Apell, N., Tropea, C., Roisman, I. V., Hussong, J., 2021, in Institute for Liquid Atomization and Spray Systems, ed., Proceedings of the 15th International Conference on Liquid Atomization & Spray Systems, volume 1, p. 96.

[8] The International Association for the Properties of Water and Steam, IAPWS R7-97(2012): Revised release on the IAPWS industrial formulation 1997 for the thermodynamic properties of water and steam.

[9] The International Association for the Properties of Water and Steam, IAPWS R12-08: Release on the IAPWS formulation 2008 for the viscosity of ordinary water substance.

[10] The International Association for the Properties of Water and Steam, IAPWS R1-76(2014): Revised release on surface tension of ordinary water substance.

[11] VDI-Gesellschaft Verfahrenstechnik und Chemieingenieurswesen, ed., 2013, VDI-Wärmeatlas, Springer, Berlin, Heidelberg.

[12] Cheng, N.-S., 2008, *Industrial & Engineering Chemistry Research - IND ENG CHEM RES*, 47 pp. 3285–3288.

[13] Yarin, A. L., 1993, Free liquid jets and films: Hydrodynamics and rheology, Interaction of mechanics and mathematics series, Longman Scientific & Technical, Harlow, Essex.

[14] Anderson, J. D., 1990, Modern Compressible Flow: With Historical Perspective, McGraw-Hill series in aeronautical and aerospace engineering, McGraw-Hill, New York, 2. ed. edition.

[15] Vogl, N., Odenthal, H.-J., Hüllen, M., Luh, M., Roisman, I. V., Tropea, C., 2019, in Steel Institute VDEh, ed., Proceedings of the 4th European Steel Technology and Application Days.

[16] Urionabarrenetxea, E., Avello, A., Rivas, A., Martín, J. M., 2021, *Materials & Design*, 199 p. 109441.

[17] Lubanska, H., 1970, *JOM*, 22 (2) pp. 45–49.